

# Using Quantum Entangled Photons to Measure the Absolute Photon Detection Efficiency of a Multi-Pixel SiPM Array

J.O.D Williams<sup>a,\*</sup>, J.S. Lapington<sup>a</sup>, S.A. Leach<sup>a</sup>, C. Duffy<sup>a</sup>

<sup>a</sup>*Department of Physics and Astronomy, University of Leicester, Leicester, United Kingdom*

---

## Abstract

Spontaneous parametric down-conversion (SPDC) of a visible pump photon is the generation of two less energetic, quantum entangled photons (QEPs), often in the near infrared (NIR), using a non-linear crystal e.g. beta barium borate. Since the detection of one QEP predicates the existence of its entangled twin, QEPs have previously been used to measure the absolute photon detection efficiency (PDE),  $\eta(\lambda)$ , of a detector under test by measuring time-coincident events with an additional trigger detector, allowing evaluation of  $\eta_{DUT}(\lambda)$  without recourse to a calibrated reference detector. In this paper, the QEP absolute PDE measurement technique is outlined, and an extension of this technique is proposed to measure  $\eta(\lambda)$  for pixels on a multi-pixel array where each pixel provides an individual signal output. By treating all pixels in a multi-pixel array as indistinguishable, Monte Carlo simulations show that the symmetry of the measurement allows  $\eta(\lambda)$  to be determined for each pixel. A route towards experimental measurements using this technique with a 64-pixel SiPM array combined with a 64-channel waveform digitiser module is outlined.

*Keywords:* Silicon photomultiplier, SiPM, Quantum Entanglement, Photon Detection Efficiency

*PACS:* 85.60.Gz, 85.60.Ha, 29.40.Ka

---

## 1. Introduction

Photon detection efficiency (PDE) describes the proportion of photons incident on a detector that cause a photoresponse, an important figure of merit for photodetectors. Determining the absolute PDE is a complex measurement that requires a well characterised, stable light source and a wavelength calibrated detector; at visible wavelengths, a typical method is to use a laser diode and a calibrated photodiode [1].

An alternative technique uses a non-linear crystal to down-convert one pump photon to two less energetic, daughter quantum-entangled photons (QEP) that then strike two independent detectors [2, 3]. The ratio of the events incident on the two detectors can then be used to determine the absolute PDE.

In this paper, the technique is expanded to enable self-calibration of a multi-pixel detector array, where the electronics provides  $\approx$ ns timing to identify a QEP from background noise signal, and then the signal from each pixel can be extracted independently to calculate the absolute PDE of each individual pixel. Firstly, we model the technique using Monte Carlo

(MC) simulations, and then outline our ongoing route to experimental verification. This technique could provide the basis for laboratory or field-based absolute PDE measurements without reliance on the calibration and stability of a reference detector.

## 2. Spontaneous Parametric Down Conversion, Quantum Entangled Photons and Absolute PDE

Non-linear optical phenomena occur when the polarisation density of a medium does not relate linearly to the source intensity [4]. This occurs in crystals of materials such as beta barium borate (BBO) [5], potassium titanyl phosphate (KTP) [6] or LiNbO<sub>3</sub> [7]. Non-linear media can produce different optical effects [8], e.g. upconverting low energy photons into a single higher energy photon via second- and third-harmonic generation (SHG and THG, respectively), illustrated in figure 1a.

Some non-linear crystals also act as downconverters, via spontaneous parametric down conversion (SPDC)[9]. In SPDC, a single incident pump photon with a wavelength  $\lambda_{pump}$  is down converted to two daughter QEPs with a wavelength  $\lambda_{QE} \approx 2\lambda_{pump}$ . Each non-linear crystal operates at a different  $\lambda_{pump}$ ; for BBO, SPDC occurs for  $\lambda_{pump} = 355\text{nm}, 405\text{nm}, 532\text{nm}$  and

---

\*Corresponding author

Email address: jodw1@le.ac.uk (J.O.D Williams)

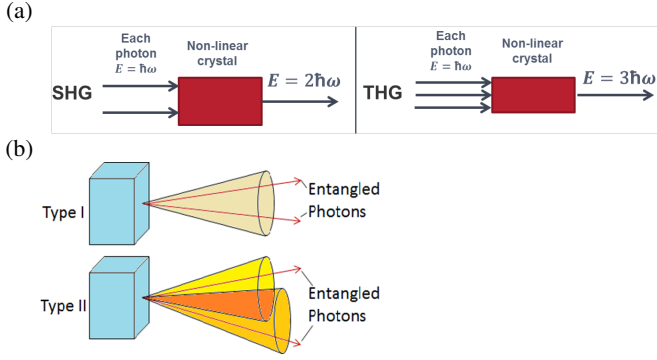


Figure 1: (a) The mechanism for second- and third-harmonic generation (SHG and THG), respectively. (b) The difference between Type I and Type II SPDC

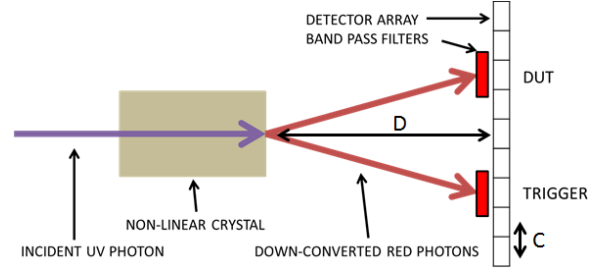


Figure 2: Experimental layout, with a pump photon  $\lambda_{Pump} \approx 350\text{nm}$  down converting to two daughter photons of  $\lambda_{DC} = 2\lambda \approx 700\text{nm}$ . Band pass filters placed in front of the detector, a distance  $D$  from the crystal, ensure that event only occurs because of two identical photon energies on symmetric pixels, with a pixel centre-centre distance  $C$ . DUT and Trigger signals are then post-processed.

775nm [10], resulting in down converted photons in the near infrared (NIR). SPDC is classified as type I or type II, depending on whether the daughter QEPs are ordinarily or extraordinarily polarised, which constrains the direction of the emitted photons, figure 1b. QEPs are emitted at a characteristic angle relative to the optical axis: BBO crystals produce a photon ring, while BiBO produces an oval [11]. SPDC is an inefficient process, generating QEPs at a rate of 4 in  $10^6$  in BBO [11]. Non-interacting pump photons could lead to other effects (e.g. SHG) or pass through the crystal without interacting. A band pass filter can be used to block these excess photons, subject to band pass transmission of typically  $\approx 1$  in  $10^4$  for a Fabry-Perot filter.

The generation of two QEPs via SPDC has been identified as a route to determine the absolute PDE of a photodetector. The entangled photon pair strikes two separate detectors, one a detector under test (DUT), and the other a "trigger" [3]. As they are entangled, a detection by the trigger detector ensures that a photon is also present at the DUT. The number of photons detected by each detector is given by

$$N_{Trigger, DUT} = \eta_{Trigger, DUT} N \quad (1)$$

where, for each detector,  $N$  is the incident number of photons,  $N_{Trigger, DUT}$  is the detected number of photons, and  $\eta_{Trigger, DUT}$  is the absolute PDE. The number of photons detected by both detectors simultaneously,  $N_{Coinc}$ , is therefore given by

$$N_{Coinc} = \eta_{DUT} \eta_{Trigger} N \quad (2)$$

Using equations 1 and 2,  $\eta_{DUT}$  is shown to be

$$\eta_{DUT} = N_{Coinc} / N_{Trigger} \quad (3)$$

Here,  $\eta_{Trigger}$  is not required to calculate  $\eta_{DUT}$  - only the number of coincident events on both detectors and the number of events detected only on the trigger detector are required.

### 3. Concept

This technique can be extended to characterise all pixels on a multi-pixel array, figure 2. As the trigger and DUT detectors are indistinguishable, the system is symmetric and calculation of  $\eta$  can be undertaken for both detectors simultaneously. This

could provide the basis for a simple to use laboratory-based tool for absolute PDE characterisation of multi-pixel arrays.

An MC simulation was developed to determine the effect of the crystal-to-detector distance,  $D$ , and band pass filter bandwidth,  $B$ , for a pump photon of energy  $E$  and momentum  $p$  incident on a BBO crystal. The MC simulation was also used to determine the procedure required to measure the absolute PDE.

#### 3.1. Monte Carlo Simulation Setup

In the MC simulation, photons were incident on a BBO crystal, of which 4 in  $10^6$  generated QEP pairs via SPDC. Each QEP was emitted at angles  $(\Theta, \phi)$  relative to the optical axis, figure 3.  $\Theta$  and  $\phi$  were randomly selected;  $\Theta$  was selected by  $\Theta = \theta + \delta\theta \approx 3.5^\circ \pm 0.25^\circ$  [11, 12]. As this setup used a type I BBO crystal,  $\Theta(\phi)$  was constant [11].

$\Theta$  and  $\phi$  were used to determine the pixel coordinate on the x-y plane where each daughter photon impacted the detector array, figure 3. A simplified SiPM detector, made up of 11x11 pixels, was used to aid computation time. Each pixel comprised 10 microcells and was allocated  $N_{-5}$  to  $N_5$ . Given  $\Theta$  and  $\phi$ , the individual photon energy and momentum components,  $E_i$  and  $p_i$ , were calculated. A band pass filter, with a central wavelength  $\lambda_{central} = 810\text{nm}$  and a band pass width  $B = 0-10\text{nm}$ , restricted  $\lambda_{QE}$  and the position where QEPs strike the detector.

Any pump photons that did not generate QEP pairs via the BBO crystal were assumed to strike the band pass filter. Of these, 1 in  $10^4$  leaked through the band pass filter and struck the central pixel, pixel  $N_0$ .

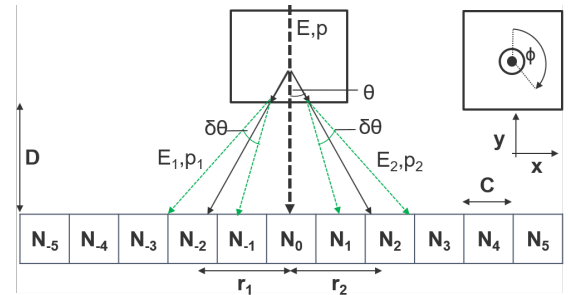


Figure 3: The arrangement used for the MC simulation.  $\Theta$  (left) and  $\phi$  (right) values were randomly selected for each run. The energy and momentum of each photon was calculated to determine where it would strike the detector.

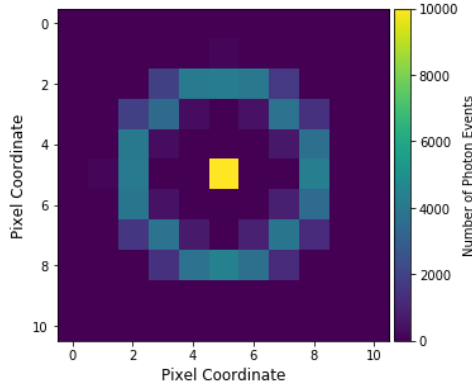


Figure 4: The ring that forms without a band pass filter, with  $\approx 4000$  events in any one pixel in the ring, and  $10^9$  events in the central spot.  $D=500$  microcells.

### 3.2. Monte Carlo Simulation Results

Initial MC simulations shows that a ring is formed where the daughter QEPs are incident on the SiPM array, figure 4, as expected from ref. [11]. There is also a high intensity central spot, where non-SPDC photons strike the SiPM array. Assuming that there is an independent signal for each pixel, we can discriminate against the central pixel signal.

A band pass filter was inserted to filter out all but the QEP photons as far as possible. The width of the band pass filter,  $B$ , dictates how close  $\lambda_{QE}$  must be to  $\lambda_{central}$ , and thus the number of photons that pass through the band pass filter and strike the SiPM array. In the MC simulation, for  $D=500$  microcells, a wider band pass filter results in a decrease in the apparent attenuation of the number of daughter photons in a particular pixel, varying from  $\approx 97\%$  for a 5nm wide band pass filter to  $\approx 65\%$  for a 40nm wide band pass filter as shown in figure 5a. Therefore the selection of band pass filter is a trade off between the number of daughters that are generated, with a greater number decreasing statistical error, versus ensuring that detected photons are daughter photons, entangled and of equal energy.

Furthermore, any individual pixel(s) can be characterised simply by changing the crystal to detector distance,  $D$ , or by moving where the pump photons are focussed. The total number of photons incident on each microcell is shown in figure 5b, with and without a 5nm wide band pass filter, for  $D$  in units of the microcell size. There is a significant decrease in the number of events that pass through the band pass filter cf. without the band pass filter. These must come from unequal photon energy events or, equivalently, false-positive entanglement events, which makes the band pass filter crucial. However, with increasing  $D$ , the intensity of events per pixel decreases due to the spread of events from  $\Theta$  and  $\phi$ , such that each pixel covers a smaller fraction of  $2\pi$ . As a result, obtaining a certain number of events in a particular pixel may take longer for greater  $D$ .

### 3.3. Determining the Pixel Absolute PDE

In a further MC simulation, each pixel was allocated an absolute PDE between 0 and 5%. If a generated photon passed through the band pass filter, a random number  $R=(0,1)$  was selected and compared to the pixel PDE to determine if the event

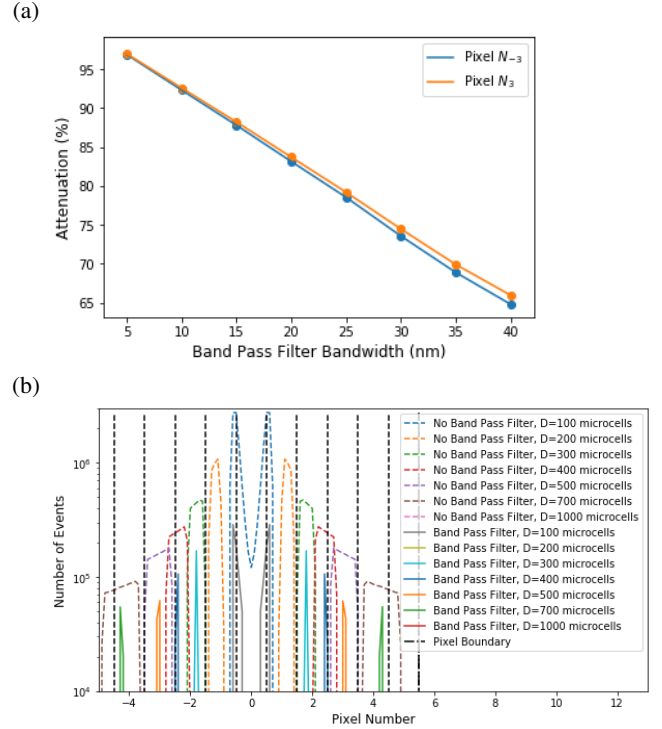


Figure 5: (a) The attenuation of the number of photon events on a given pixel with a band pass filter of a specific bandwidth compared to no band pass filter at all.  $10^6$  runs. (b) The number of photon events registered in each pixel, with and without a 5nm wide band pass filter. There is a large decrease in counts for each pixel with the band pass filter, due to false-positive entanglement events.

registered on the corresponding microcell, as happens implicitly in a SiPM. The numbers of events in each microcell, for  $D=200$  and 400 microcells, was summed to quantify the total number of events per pixel, while events where both photons registered were also counted for each pixel. Each pixel absolute PDE was then calculated via equation (3), and plotted against the original stated PDE, figure 6. In this case, the MC model suggests that the absolute PDE can be measured to an accuracy of  $\pm 12\%$  in 65% of pixels, and  $\approx \pm 25\%$  in 82% of pixels. Some of the less accurate measurements arise due to low event SPDC events in the pixels further from the central spot.

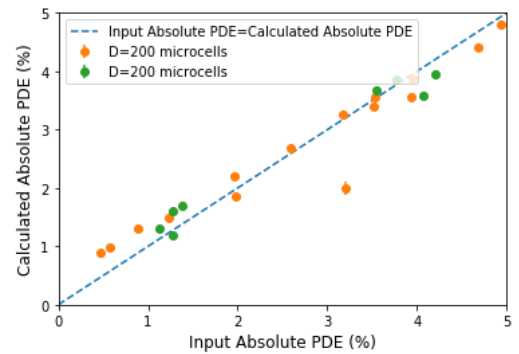


Figure 6: Calculated absolute PDE from each individual pixel compared to the stated absolute PDE used for the MC simulations.  $D=200$  and 400 microcells, for  $10^7$  and  $10^8$  QEPs incident across the array respectively. The dashed line shows the case where the calculated PDE equals the input PDE.

## 4. Route to Experimental Verification

To achieve verification of this technique with a multi-pixel array, the experimental setup requires:

1. single photon resolution with photon timing on a nanosecond timescale. Given the low SPDC rate, down conversion events per pulse will produce single photons.
2. individual outputs from each pixel, to enable the pixel response (e.g. time of peak) to be analysed.
3. high sample rate. Timing  $\leq 1\text{ns}$  enables correlated photons to be identified, while reducing the possibility of false-positive correlated photons.

### 4.1. Electronics

Tests are on-going with a Hamamatsu S12642 SiPM array of 64 6mm x 6mm pixels connected to a TARGET module, developed for the CHEC-S camera, a candidate camera for the Cherenkov Telescope Array [13]. Each pixel is connected to a 64 channel 1GHz digitiser, based on the TARGET ASIC [14], designed for fast timing and coincidence measurements. Optimisation of the TARGET module setup, including array cooling and calibration of the electronics, enables single photon resolution with a timing accuracy  $< 2\text{ns}$ . Each channel can be analysed to determine the number of correlated photon events between any two pixels where QEPs struck the detector array.  $\eta_{DUT}$  can then be calculated for the array, including pixel dead space.

### 4.2. Achieving Spontaneous Parametric Down Conversion

To achieve SPDC, a 5mm diameter BBO Type-I crystal is illuminated by a Photek LPG-1 pulsed laser with a peak emission at 405nm. Down converted photons emitted by the BBO crystal then pass through a band pass filter ( $\lambda_{\text{central}}=810\text{nm}$ ,  $B \approx 10\text{nm}$ ). The experimental setup is shown in figure 7a.

In our initial results, photons within a given arrival time (32-38ns) and signal window (3-12mV) are counted for each pixel, figure 7b. The time and signal window ensures that dark noise contributions are minimised and that each photon event is only 1-2 photons, although optical crosstalk means that some events may be missed [15]. Work is on-going to verify that this ring is due to SPDC-events, and not from reflections of the laser within the optical arrangement or other structured sources of noise.

## 5. Conclusion

In this paper, the original technique to use quantum entangled photons to characterise the absolute PDE of a detector has been extended to characterise SiPMs in a multi-pixel array. This setup allows for all pixels in an array to be characterised without the requirement for a well calibrated photodiode and/or detector, and utilises the system symmetry so that trigger and DUT pixels can be characterised simultaneously. Monte Carlo simulations have shown that this technique can provide a good estimate of the pixel PDE, and can characterise any pixel by varying  $D$  and the location of the central pixel,  $N_0$ .

To achieve this technique experimentally, it requires a low noise system, fast timing and individual pixel outputs. Ongoing

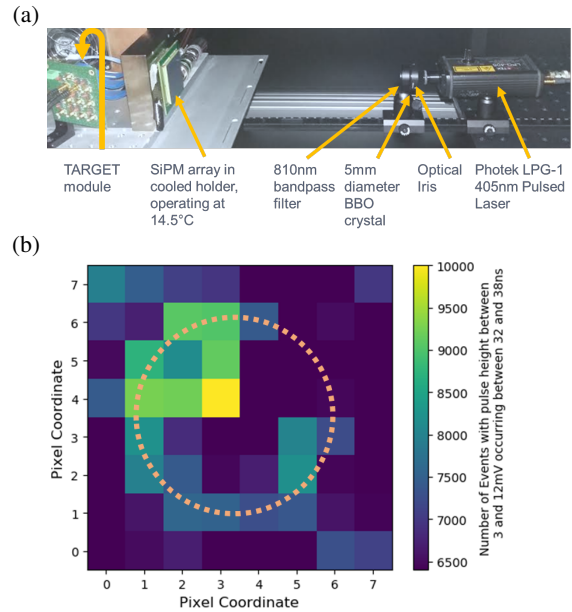


Figure 7: (a) Experimental setup, comprising a pulsed laser, optical iris, BBO crystal, band pass filter, SiPM array and TARGET module. (b) A ring produced by BBO, indicated by a dashed line, with a central spot within the ring. Four dead pixels in the top right of the array prevent the full ring being observed.

experiments are using a 64-channel 1GHz waveform digitiser, a Hamamatsu SiPM array and daughter photons produced at 810nm. This technique uses readily-available laboratory equipment and could, therefore, provide the basis for a simple, low-cost tool for absolute PDE characterisation in a laboratory.

## References

- [1] A. Nagai, et al, SENSE: A comparison of photon detection efficiency and optical crosstalk of various SiPM devices, Nucl Instrum Methods Phys Res A, (2017)
- [2] A. Migdall, et al, Intercomparison of a correlated photon-based method to measured detector quantum efficiency, Appl Optics, 41, 15 (2002)
- [3] M. Ware and A. Migdall, Single-Photon detector characterisation using correlated photons: the march from feasibility to metrology, J Mod Optic, 51, 9-10 (2004) 1549-1557
- [4] R. Boyd, Nonlinear Optics, Academic Press (2008)
- [5] D.N. Nikogosyan, Beta Barium Borate, Appl Phys A-Mater, 52, 6 (1991)
- [6] S. Dezhong and H. Choaeon, A New Non-Linear Optical Crystal KTP, Prog. Crystal Growth and Charact., 11 (1985) 269-274
- [7] G.D. Boyd, et al, LiNbO3: An Efficient Phase Matchable Nonlinear Optical Material, Appl Phys Lett, 5, 11, (1964), 234
- [8] F. Trager, Handbook of Lasers and Optics, Springer, (2007)
- [9] T.E. Kiess, et al, Einstein-Podolsky-Rosen-Bohm experiment using pairs of light quanta produced by type-II parametric down-conversion, Phys Rev Lett, 71 (1993) 3893
- [10] New Light Photonics, Available: <http://www.newlightphotonics.com/SPDC-Components/BBO-SPDC-Crystals>, (2018)
- [11] H.E. Guilbert, et al, Observation of elliptical rings in type-I spontaneous parametric downconversion, J Opt Soc Am B, 32, 10 (2015), 2096-2103
- [12] S.Y. Baek and Y.H. Kim, Spectral properties of entangled photon pairs generated via frequency-degenerate type-I spontaneous parametric down-conversion, Phys Rev A, 77 (2008)
- [13] J.S. Lapington, et al, The GCT camera for the Cherenkov Telescope Array, Nucl Instrum Methods Phys Res A, 876 (2017), 1-4
- [14] S. Funk, et al, TARGET: A Digitizing and Trigger ASIC for the Cherenkov Telescope Array, AIP Conf Proc, 1792 (2017)
- [15] J.O.D Williams, et al, A normally-distributed crosstalk model for silicon photomultipliers, Nucl Instrum Methods Phys Res A, (2018)